

Calculating Thermodynamic Properties from Fluctuations at Small Scales

Sondre K. Schnell,[†] Xin Liu,^{†,‡} Jean-Marc Simon,[§] André Bardow,[‡] Dick Bedeaux,^{||} Thijs J. H. Vlugt,[†] and Signe Kjelstrup^{*†,||}

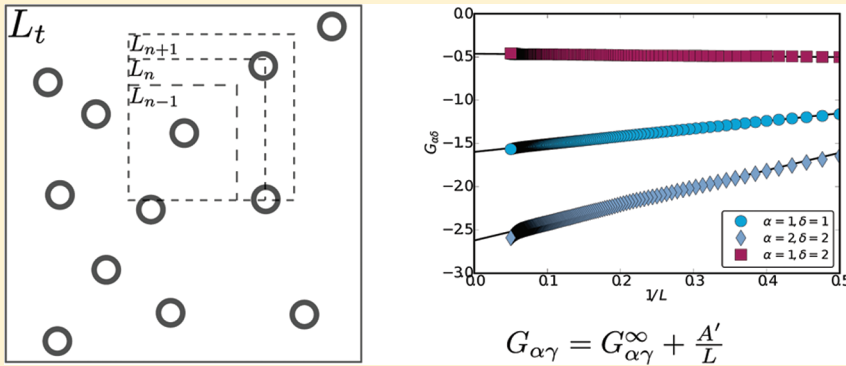
[†]Process and Energy Laboratory, Delft University of Technology, Leeghwaterstraat 44, 2628CA Delft, The Netherlands,

[‡]Lehrstuhl für Technische Thermodynamik, RWTH Aachen University, Schinkelstraße 8, 52062 Aachen, Germany

[§]Laboratoire Interdisciplinaire Carnot de Bourgogne, UMR 5209 CNRS-Université de Bourgogne, Dijon, France, and

^{||}Department of Chemistry, Norwegian University of Science and Technology, Trondheim, Norway

ABSTRACT:



We show how density and energy fluctuations of small nonperiodic systems embedded in a reservoir can be used to determine macroscopic thermodynamic properties like the enthalpy density and the thermodynamic correction factor. For mixtures, the same formalism leads to a very convenient method to obtain so-called total correlation function integrals, also often referred to as Kirkwood–Buff integrals. Using finite size scaling, the properties obtained for small systems can be extrapolated to the macroscopic system limit provided that the system is sufficiently far from the critical point. As derived in our previous work (*Chem. Phys. Lett.* 2011, **504**, 199–201), the finite size scaling is significant and depends on $1/L$, where L is the length of the small system in one dimension. By considering a reservoir with an ensemble of embedded small systems, we can use the scaling arising from surface effects to determine properties for macroscopic systems by extrapolation. We demonstrate this method for the WCA and LJ fluids, as well as for a heterogeneous system, i.e., argon adsorbed in silicalite-1 zeolite.

1. INTRODUCTION

Until recently, thermodynamics of nanoscale systems has not received much attention. The problem when these systems are studied is the small scale. Systems at the nanometer scale are difficult to handle experimentally, and so far the thermodynamics of such small systems has not been the focus of investigations in nanoscience. It is important to note that small systems are strongly influenced by surface effects, which cannot be neglected.¹ In principle, these surface effects could be exploited in practical applications or theory/simulations. With this in mind, it becomes important to find a consistent framework describing the thermodynamics of small systems. A theoretical formulation of thermodynamics of small systems is for example given by Hill.² The crucial difference between small systems and macroscopic systems is that the enthalpy and Gibbs energy are no longer extensive. Therefore, thermodynamic properties obtained for small systems cannot be directly compared to thermodynamic properties of macroscopic systems.

In a recent paper,³ we investigated the finite size scaling of small nonperiodic systems embedded in a large periodic reservoir that itself is simulated in the grand-canonical ensemble. These small nonperiodic systems can exchange particles and energy with the reservoir, similar to a system in the grand-canonical ensemble. On the basis of the formalism of Hill,² we found that thermodynamic properties attributed to the small system have a finite size scaling proportional to $1/L$, L being the length of the system in one dimension. The crucial difference with the more conventional finite-size scaling⁴ is that an effective surface energy needs to be added to account for the different boundary conditions of small periodic and nonperiodic systems.³ The predicted $1/L$ scaling was confirmed using Monte Carlo simulations in which small systems were embedded in a large simulation

Received: May 10, 2011

Revised: July 14, 2011

Published: August 12, 2011

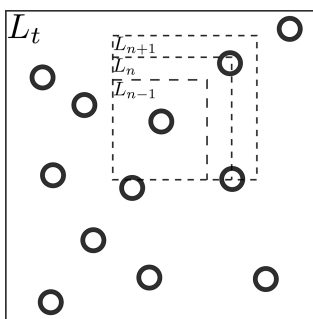


Figure 1. Sampling of small nonperiodic systems in a (periodic) simulation box (reservoir). The reservoir itself has sides of L_t in each dimension. We embed a small system by randomly selecting randomly positioned subvolumes of size L_{n-1}^d , where d is the dimensions of the system ($d = 3$ for all cases in this work). By systematically increasing the size of the subvolume (L_n, L_{n+1}), we can obtain macroscopic thermodynamic properties.

box, where the large simulation box itself was kept in the grand-canonical (μVT) ensemble. We determined the enthalpy density h and the thermodynamic correction factor Γ for small homogeneous systems. The enthalpy density h is of particular interest when studying adsorption properties.⁵ The thermodynamic correction factor Γ for a single-component system is defined by $1/\Gamma = k_B T (\partial \ln \bar{N}/\partial \mu)_{T,V}$ in which \bar{N} is the average number of particles and μ is the chemical potential. For mixtures, Γ is related to deviations from ideal mixture behavior and this quantity is commonly used to relate Fick and Maxwell–Stefan diffusivities.^{6,7} By integrating the thermodynamic correction factor Γ over the chemical potential, we can obtain the adsorption isotherm (number of molecules as a function of the chemical potential).⁸ This is applicable when the adsorption of small guest molecules in microporous materials such as zeolites or MOFs is studied.⁹

The process of embedding a small system inside a large reservoir is shown in Figure 1. The large system with sides L_t (in each dimension) is simulated with periodic boundary conditions. Several small systems embedded in the reservoir (denoted by L_{n-1}, L_n , and L_{n+1}) can exchange energy and particles with the large reservoir. When the large system L_t is in the grand-canonical ensemble, the small systems will be too. If the reservoir is in another ensemble (e.g., NVT or NPT), the small systems are only in the grand-canonical ensemble when $L_n \ll L_t$. By considering the scaling of small system properties with the size of the small system, we are able to extract macroscopic thermodynamic properties. In the present study, we show that this method is very efficient for obtaining total correlation function integrals, also referred to as Kirkwood–Buff (KB) integrals.¹⁰ Partial molar volumes, the compressibility, and partial derivatives of activity coefficients can be obtained from single molecular dynamics (MD) simulations by computing KB integrals. It is important to note that in the thermodynamic limit the choice of ensemble for the large reservoir is irrelevant.¹¹ Thus, our method provides a unique way of accessing the grand-canonical ensemble without having to rely on particle insertions and deletions, which can be extremely inefficient for dense systems.^{11,12} Sufficiently large systems with periodic boundary conditions simulated in the grand-canonical ensemble¹¹ were used to obtain reference values for thermodynamic properties in the thermodynamic limit.

The remainder of this paper is organized as follows: in section 2 we show how various thermodynamic properties can be computed using the proposed scaling. In section 3, we describe

the simulation method, as well as the systems that were studied in this work. Results for homogeneous and inhomogeneous systems (i.e., argon adsorbed in silicalite-1) are shown in section 4, and in section 5 our findings are summarized.

2. SMALL SYSTEM SCALING TO OBTAIN THERMODYNAMIC PROPERTIES

We consider a d -dimensional small system as a subvolume of a larger system (reservoir) (Figure 1). The sizes of these systems in one dimension are denoted by L_n and L_t , respectively. The small system and the reservoir can exchange energy and particles. As the small system shares a surface with the reservoir, an effective surface energy $E^s(\mu, T)$ needs to be taken into account in a thermodynamic description of the small system. This effective surface energy originates from the difference between a small nonperiodic system and a system with periodic boundary conditions.³ Using the theory of Hill,² we previously derived the following equations for the scaling of thermodynamic properties of embedded one-component small systems³

$$\frac{1}{\Gamma} = 1 + \frac{2d\Lambda}{L} \left[\frac{\partial E^s}{\partial \mu} \left(1 + \frac{\partial E^s}{\partial \mu} \right) + \frac{\partial^2 E^s}{\beta \partial \mu^2} \right] \exp(\beta E^s) \\ = \frac{1}{\Gamma_\infty} + \frac{C'}{L} \quad (1)$$

$$\bar{h} = \frac{\bar{H}}{V} = \left(1 + \frac{d}{2} \right) k_B T \Lambda^{-d} \exp(\beta \mu) \\ + 2d \left(\frac{d+1}{2} k_B T - E^s + T \frac{\partial E^s}{\partial T} + \mu \frac{\partial E^s}{\partial \mu} \right) L^{-1} \Lambda^{1-d} \\ \times \exp(\beta(E^s + \mu)) = h_\infty + \frac{B'}{L} \quad (2)$$

where Γ is the thermodynamic correction factor, \bar{h} is the enthalpy density, L is the length of the system in one dimension, and B' and C' are constants that do not depend on L . The subscript ∞ denotes macroscopic properties. In addition, we have $\beta = 1/k_B T$, where k_B is the Boltzmann constant, T is the absolute temperature, μ is the chemical potential, \bar{H} is the average enthalpy, V is the volume, and Λ is the mean thermal de Broglie wavelength. Equations 1 and 2 are independent of the dimensionality of the system when we are using L instead of the volume ($L = V^{1/d}$, where d is the dimensionality).

2.1. Pure Component Systems. The thermodynamic correction factor and the enthalpy follow from density and energy fluctuations in the grand-canonical ensemble. For single component systems, these can be described as^{7,13}

$$\frac{1}{\Gamma} = k_B T \left(\frac{\partial \ln \bar{N}}{\partial \mu} \right)_{T,V} = \frac{\langle N^2 \rangle - \langle N \rangle^2}{\langle N \rangle} \quad (3)$$

$$h = - \frac{\langle UN \rangle - \langle U \rangle \langle N \rangle}{\langle N^2 \rangle - \langle N \rangle^2} \quad (4)$$

where the brackets $\langle \dots \rangle$ denote an ensemble average in the grand-canonical ensemble, N is the number of particles, U is the potential energy, and h is the enthalpy density. The molar energy is proportional to the enthalpy density. For homogeneous

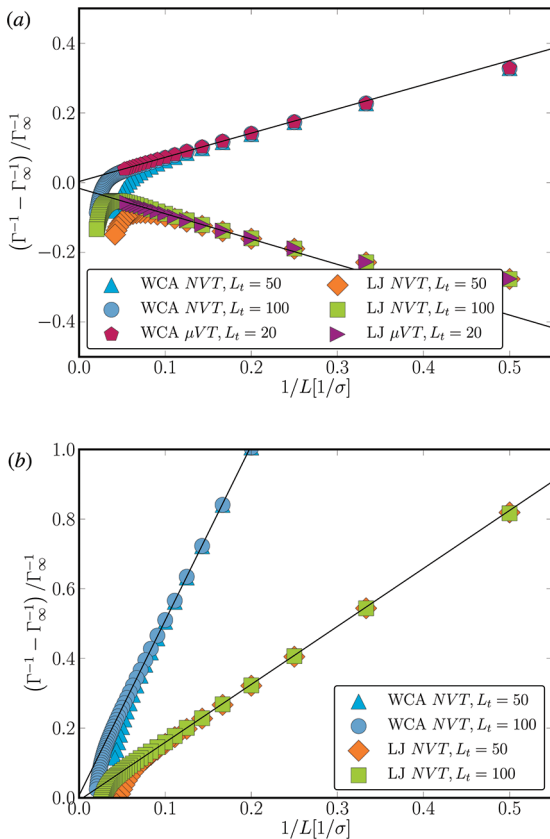


Figure 2. Inverse thermodynamic correction factor for the WCA and LJ fluids at reduced densities of (a) $\rho^* = 0.15$ and (b) $\rho^* = 0.60$. The temperature is $T^* = 1.8$ in reduced units. In (a) we also added the points obtained from sampling small systems in a reservoir equilibrated in the grand-canonical ensemble. The data obtained from the grand-canonical ensemble follow the straight lines well, whereas the data obtained from canonical reservoirs show deviations from linearity when $1/L \rightarrow 0$. This is a result of the reservoir being too small compared to L , as it no longer serves as a μT reservoir. We obtained the reference value Γ_{∞}^{-1} from the simulation in the grand-canonical ensemble using periodic boundary conditions.

systems, the molar enthalpy is used, whereas for inhomogeneous systems (e.g., argon in silicalite-1) the molar isosteric heat of adsorption q_{st}^* can be obtained directly from h .¹³ The isosteric heat of adsorption of argon is defined as the enthalpy change when argon is adsorbed from the gas phase into the host structure.^{5,13}

2.2. Binary and Multicomponent Systems. Thermodynamic properties of mixtures can be obtained from total function correlation integrals, also referred to as Kirkwood–Buff (KB) integrals. This so-called fluctuation solution theory, derived a long time ago by Kirkwood and Buff,¹⁰ relates fluctuations in the grand-canonical ensemble to integrals of radial distribution functions over the volume:

$$G_{\alpha\delta} = V \frac{\langle N_{\alpha}N_{\delta} \rangle - \langle N_{\alpha} \rangle \langle N_{\delta} \rangle}{\langle N_{\alpha} \rangle \langle N_{\delta} \rangle} - \frac{\delta_{\alpha\delta}}{c_{\alpha}} \quad (5)$$

$$= 4\pi \int_0^{\infty} [g_{\alpha\delta}^{\mu VT}(r) - 1] r^2 dr \quad (6)$$

$$\approx 4\pi \int_0^R [g_{\alpha\delta}^{NVT}(r) - 1] r^2 dr \quad (7)$$

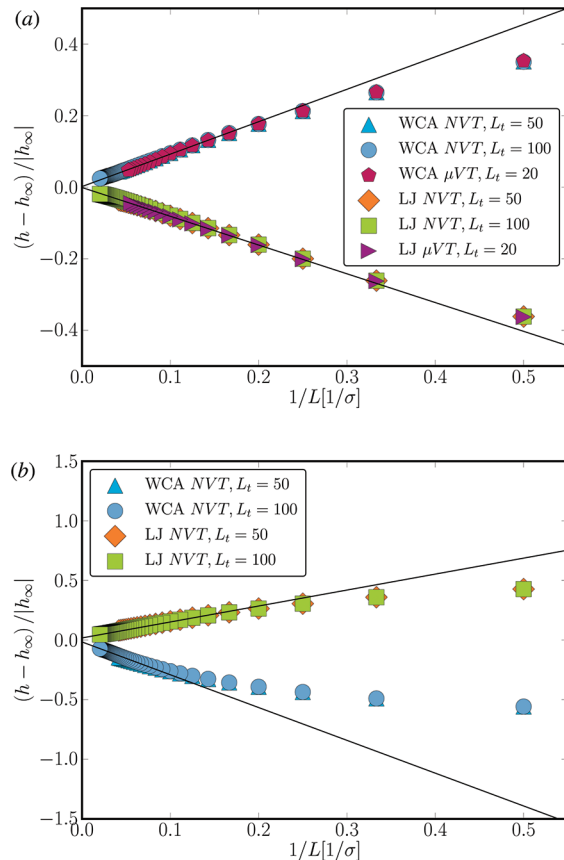


Figure 3. Enthalpy density from a system with reduced density of (a) $\rho^* = 0.15$ and (b) $\rho^* = 0.60$. The temperature is $T^* = 1.8$ in reduced units. From the figures, we clearly see that the molar heat of adsorption is less sensitive to the size of the reservoir than the thermodynamic correction factor. We obtain the value for h_{∞} from simulations in the grand-canonical ensemble using periodic boundary conditions.

in which the value of the integration limit R should be sufficiently large. In these equations, averages in the grand-canonical ensemble are denoted by the brackets $\langle \dots \rangle$, $g(r)$ is the radial distribution function, V is the volume, N_{α} is the number of particles of component α , $\delta_{\alpha\delta}$ is the Kronecker delta and $c_{\alpha} = \langle N_{\alpha} \rangle / V$ is the concentration of component α . The approximation $g_{\alpha\delta}^{NVT}(r) \approx g_{\alpha\delta}^{\mu VT}(r)$ is nearly always safe, as all ensembles are equivalent in the thermodynamic limit. Close to the critical point, concentration fluctuations will become very long-ranged and therefore integration of $g(r) - 1$ over volume will not be possible in practice. The use of eq 7 is particularly useful at temperatures well below the critical point, where simulations in the grand-canonical ensemble suffer from poor acceptance ratios for particle insertions/removals.¹¹ Thermodynamic properties of mixtures directly follow from $G_{\alpha\delta}$, for example the partial derivative of the activity coefficient γ_1 of component 1 in a binary system equals¹⁰

$$\left(\frac{\partial \ln \gamma_1}{\partial x_1} \right)_{p,T} = \frac{\Gamma_{11} - 1}{x_1} = - \frac{c_2(G_{11} + G_{22} - 2G_{12})}{1 + c_2x_1(G_{11} + G_{22} - 2G_{12})} \quad (8)$$

where x_1 is the mole fraction of component one and Γ_{11} is an element of the matrix of thermodynamic factors.⁶ Expressions

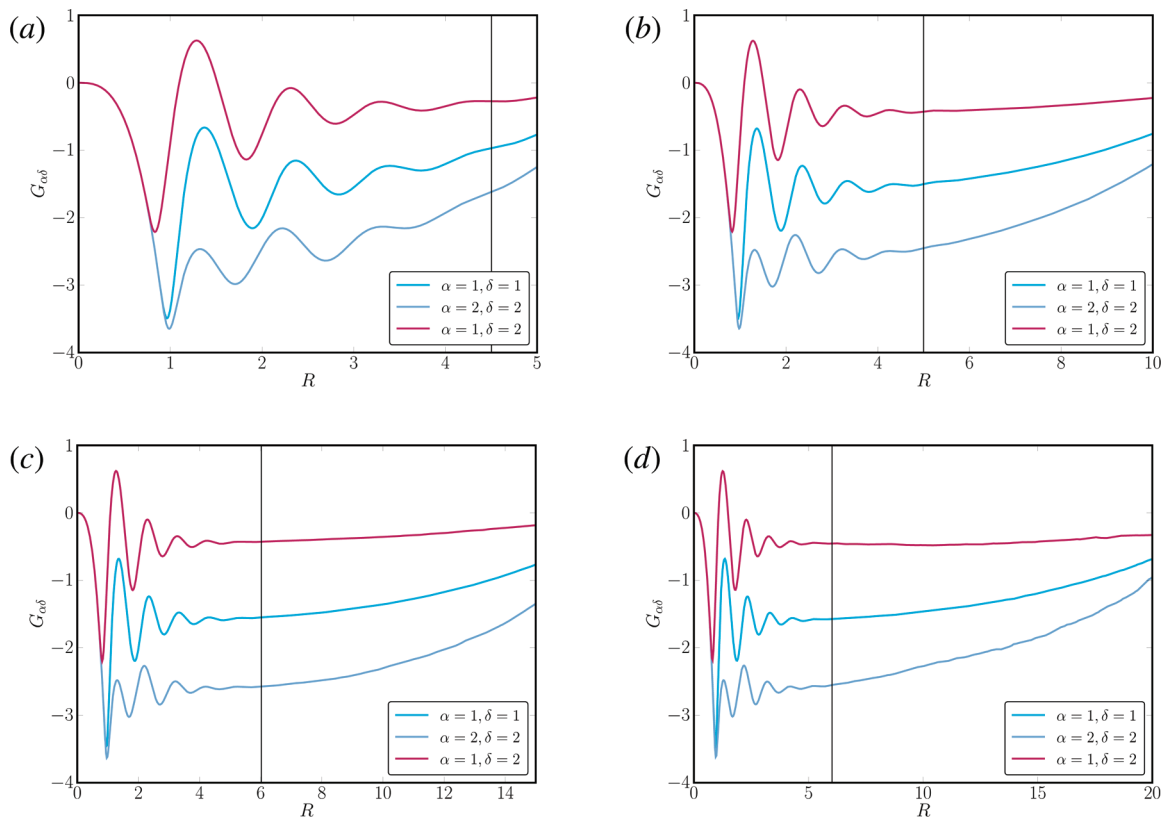


Figure 4. Kirkwood–Buff integrals for a 70/30 binary WCA system. The estimated values of $G_{\alpha\delta}$ are shown as functions of the integration boundaries (see eq 7). (a) $L_t = 10$, (b) $L_t = 20$, (c) $L_t = 30$, and (d) $L_t = 40$. For (a) and (b) it is hard to distinguish where the integral converges. For (d) we observe that $[g(r) - 1]r^2$ was not obtained sufficiently accurate for larger values of R . The vertical lines indicate where the values for $G_{\alpha\beta}$ listed in Table 1 were taken. All simulations were performed at a reduced density of $\rho^* = 0.75$ and a reduced temperature of $T^* = 1.8$.

Table 1. Values for KB Integrals $G_{\alpha\delta}$ Determined by Integrating the Radial Distribution Function (Eq 7, Figure 4), and from Extrapolating the Values Found by Embedding Small Systems (Eqs 5 and 9, Figure 5)^a

L_t/σ	$\alpha\delta$	R/σ	eq 7	eq 5, eq 9
10	11	4.503	-0.977	-1.601
	22		-1.633	-2.686
	12		-0.275	-0.440
20	11	5.000	-1.508	-1.594
	22		-2.456	-2.601
	12		-0.429	-0.464
30	11	6.023	-1.552	-1.600
	22		-2.577	-2.602
	12		-0.428	-0.461
40	11	6.027	-1.574	-1.600
	22		-2.555	-2.621
	12		-0.455	-0.463

^a The limit R for the integration of eq 7 is also given. Determining $G_{\alpha\delta}$ from the radial distribution function requires a box of at least sides $L_t = 30$ in this case. Embedding small systems and extrapolating leads to a very good estimation of $G_{\alpha\delta}$ already at $L_t = 10$, and the values are nearly identical for larger reservoirs.

for partial molar volumes, the isothermal compressibility and partial derivatives of activity coefficients in terms of KB integrals for binary and ternary systems can be found in ref 14.

It is important to note that the convergence of the integral in eq 7 using $g(r)$ obtained from molecular simulations is often poor. In practice, this integration requires extremely accurate estimates for $g(r)$ as well as very large box sizes. The reason for this is that $g(r)$ only converges to 1 for $r \rightarrow \infty$ for an infinitely large system. For a system of finite size, $g(r)$ converges to a value different from 1 when $r \rightarrow \infty$. Various approximations and interpolations may be needed for the KB integrals to converge; see, for example, the work of Wedberg et al.^{15,16} and Christensen et al.^{17,18} The latter authors also pointed out that although the individual terms $G_{\alpha\delta}$ are difficult to obtain by direct integration, partial derivatives of the activity coefficients using eq 8 for binary mixtures do not depend too much on the upper integration limit R by a lucky cancellation of errors. Such a cancellation is not present for ternary systems.¹⁴ Recently, Nichols et al.¹⁹ have proposed an improved method for the determination of $G_{\alpha\delta}$ for systems with periodic boundary conditions. Their method is based on reducing systematic errors introduced by the boundary conditions, requiring a finite-Fourier-series expansion of concentration fluctuations. Clearly, there is a considerable interest in developing more efficient methods to extract KB integrals from simulations.

3. SYSTEMS STUDIED

3.1. Homogeneous Systems. Two different interaction potentials are considered in this study: WCA and Lennard-Jones (LJ) interactions. Equations 1 and 2 provide the scaling with respect to $1/L$ for both Γ and h in small nonperiodic systems.

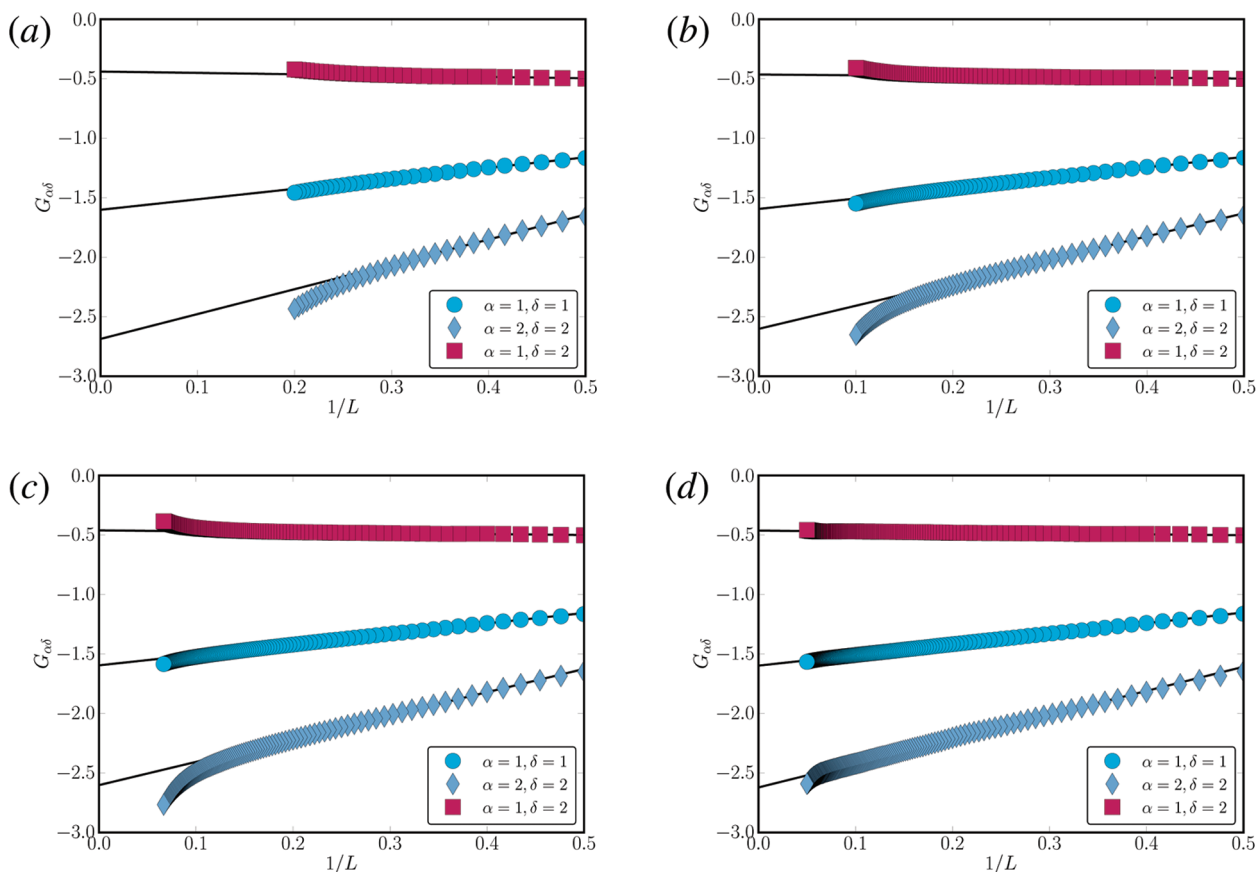


Figure 5. KB integrals for a 70/30 binary WCA system calculated using eqs 5 and 9. Finite size scaling of $G_{\alpha\delta}$ as determined from sampling small systems embedded in a large reservoir of size L_t . (a) $L_t = 10$, (b) $L_t = 20$, (c) $L_t = 30$, and (d) $L_t = 40$. We fitted straight lines to the linear regime and extrapolated until the thermodynamic limit ($1/L \rightarrow 0$). The final values of $G_{\alpha\delta}$ are shown in Table 1. The density of the system was in all cases $\rho^* = 0.75$ in reduced units, and $T^* = 1.8$.

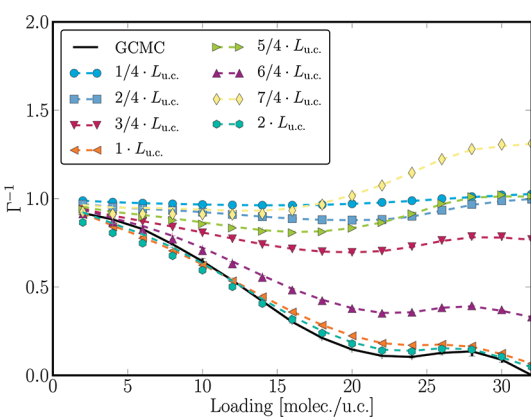


Figure 6. Thermodynamic correction factor of argon in silicalite-1, obtained by sampling with small systems in a large simulation box at $T = 100$ K. The solid line is a thermodynamic correction factor obtained from simulations in the grand-canonical ensemble using periodic boundary conditions. The dashed lines are from embedding small systems in a simulation box in the grand-canonical ensemble, and the symbols are from embedding small systems in the canonical ensemble.

The large reservoir with periodic boundaries is equilibrated in the grand-canonical or canonical ensemble. Separate grand-canonical simulations with periodic boundary conditions were used to

obtain the values for Γ and h in the thermodynamic limit (denoted by Γ_∞ and h_∞ respectively). All simulation boxes used were cubic with sides L_t . The embedded small system had the same geometric shape as the simulation box. For the LJ fluid, we used a spherical cutoff at 2.5σ , where the potential was truncated and shifted. The WCA potential is a shifted LJ potential with the attractive tail removed.²⁰ The LJ parameters σ and ε were taken as unit length and energy respectively.

We also considered mixtures consisting of different WCA particles. For simplicity, we are using a mixture of labeled particles. The pairwise interaction between particles of equal type is given by the regular WCA potential, and the interaction energies between particles of different type are scaled by a factor 1/10. We have used a mixture of 70% particles of type 1 and 30% of type 2.

Simulations were performed using either grand-canonical Monte Carlo or MD in the NVT ensemble at a reduced temperature of $T^* = 1.8$. In the latter, the instantaneous temperature is constrained by the algorithm described in ref 21. We investigated the effect on system size of the reservoir (L_t) and varied the size of the small subsystem up to $L_t/2$.

3.2. Heterogeneous System. Monte Carlo simulations in the NVT ensemble were used to study the thermodynamics of argon adsorbed in the zeolite silicalite-1 (MFI-type zeolite) at 100 K. The force field parameters for the LJ interactions between guest–guest and guest–host pairs were taken from the work

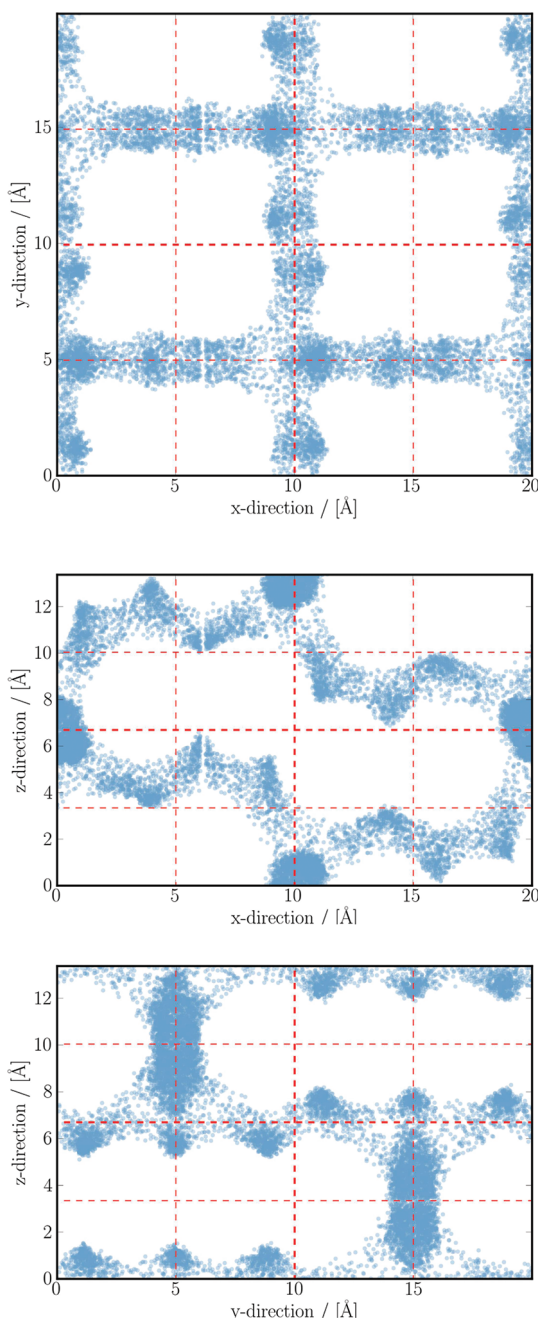


Figure 7. Positions of argon atoms inside silicalite-1 projected on the xy , xz , and yz planes. The density plots were constructed from the positions of argon in 535 snapshots, with 128 molecules per snapshot in a system with $2 \times 2 \times 2$ unit cells. One unit cell in all directions is plotted. The dashed red lines indicate the $1/4$ unit cell in each direction. We clearly see how the system is well characterized in the x and y direction with steps of $1/4$ unit cell, but the symmetry imposed by the zeolite structure requires larger steps.

of García-Pérez et al.²² All LJ interactions were truncated and shifted at 12 Å. The silicalite-1 unit cell has dimensions 20.022 Å in the x -direction, 19.899 Å in the y -direction, and 13.383 Å in the z -direction.²³ We consider a zeolite consisting of $4 \times 4 \times 8$ unit cells, leading to a simulation box with dimensions of 80.088 Å \times 79.596 Å \times 107.064 Å (128 unit cells in total). The small system sampling is identical to the sampling for the homogeneous systems, with one exception: the size of the embedded small

system was restricted to steps of $1/4$ of the crystallographic unit cell in each direction. Eight different small systems were embedded, so the largest size of a small system inserted had $8/4 = 2$ unit cells in each direction, leading a total volume of $2^3 = 8$ unit cells, which is $1/16$ th of the supercell. We varied the loading of argon from zero to the maximum loading of 32 argon molecules per unit cell, corresponding to fugacities ranging from 0.001 Pa to approximately 50 000 Pa. The thermodynamic factor and heat of adsorption computed from separate grand-canonical simulations are compared with the results from simulations in the canonical ensemble using the described fluctuation method.

4. RESULTS

4.1. Homogeneous Systems. The inverse thermodynamic correction factor Γ^{-1} for the homogeneous systems is plotted in Figure 2. The lines are straight lines fitted to the data points in the linear regime. Nook and corner effects are significant for the very small systems ($1/L > 0.5$), i.e., systems that are of the order of the size of a single particle. For very large embedded systems, we observe deviations from the linear behavior. This can be explained by the fact that the reservoir no longer can act as a grand-canonical reservoir to the embedded small system when $L \approx L_t$. For the high density system (Figure 2b), we have obtained the value for Γ_∞^{-1} from simulations in a grand-canonical ensemble, with sides $L_t = 10$ and periodic boundary conditions. This system is too small to embed small systems, but it is sufficiently large to determine Γ^{-1} for macroscopic systems from grand-canonical simulations.

Equations 1 and 2 provide the general expressions for the scaling of thermodynamic properties with $1/L$. In our previous paper,³ these equations were verified numerically when the small system was embedded in a grand-canonical reservoir. The thermodynamic correction factor was calculated in the same manner for a system with WCA particles in 2-dimensions. We have not included these results in this paper, as they do not lead to additional physical insight.

In Figure 3, we plotted the enthalpy density for WCA and LJ particles at $\rho^* = 0.15$ and $\rho^* = 0.60$. The most striking difference between the scaling of the enthalpy and the thermodynamic correction factor is the behavior of the enthalpy as the embedded system becomes large compared to the reservoir. In this case we do not see the same deviation from the linear behavior when $1/L \rightarrow 0$. This indicates that computing the enthalpy density does not require such a large reservoir as for the thermodynamic correction factor. By extrapolating from the linear regime, we are able to determine the value of h_∞ for a macroscopic system with excellent accuracy, i.e., within 1%.

In Figure 4, we plotted the KB integral $G_{\alpha\delta}$ as a function of the upper bound R (see eq 7) for a mixture of WCA particles. We investigated the effect of the system size. The vertical lines indicate the integration boundary R in each case (Table 1). The integration boundary is estimated from the plateau, which is, as expected, not always very clear as for a finite-size system $g(r)$ does not converge to 1 when $r \rightarrow \infty$ and therefore for large R the integral of eq 7 diverges. Especially for the two smallest systems (Figure 4a,b, with $L_t = 10$ and $L_t = 20$ respectively), the plateau is not easy to distinguish, suggesting that this system is too small to obtain the KB integrals. The cutoff distances as well as the values of $G_{\alpha\delta}$ for various system sizes are listed in Table 1. For larger boxes (Figure 4c, with $L_t = 30$ and Figure 4d, with $L_t = 40$), we

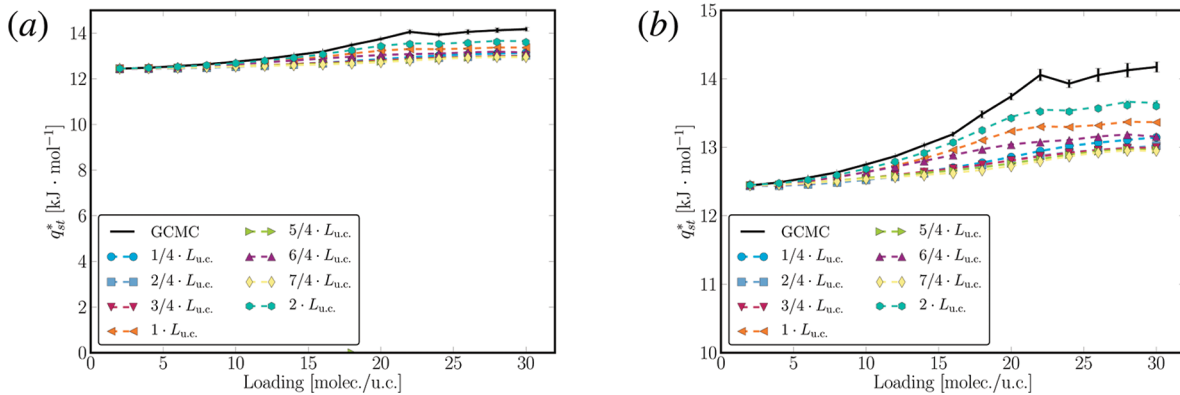


Figure 8. Isosteric heat of adsorption for argon in silicalite-1 at 100 K. The dashed lines are results from embedding small systems in a simulation box in the grand-canonical ensemble, and the symbols are from embedding small systems in the canonical ensemble. Note that (b) is a close up of (a). For this system, the shape of the control volume is not as important as for the thermodynamic correction factor. Also, we do not observe a clear finite size scaling. The heat of adsorption found from studying fluctuations lead to a very good representation of the molar isosteric heat of adsorption for this system.

find a sufficiently large plateau needed for making a reasonable estimation of the KB integrals.

In Figure 5, we plotted the values of the KB integrals when we sample the concentration fluctuations of the small systems embedded in the canonical ensemble simulation box (eq 5). In this case we expect, analogous to eqs 1 and 2 that

$$G_{\alpha\delta} = G_{\alpha\delta}^{\infty} + A'/L \quad (9)$$

in which A' is a constant that does not depend on L . The lines in Figure 5 are fitted to the linear regime. These lines are extrapolated until the intersection with the vertical axis ($1/L \rightarrow 0$), and this value is taken to be the macroscopic value of $G_{\alpha\delta}$, i.e., $G_{\alpha\delta}^{\infty}$. This value can be compared directly to the value found by integrating the radial distribution function (Table 1). An excellent agreement is observed. In all cases, we are able to distinguish the linear regime quite easily, even for relatively small systems (see Figure 5). A comparison between Figures 4 and 5 clearly shows that obtaining KB integrals from density fluctuations in subvolumes is much more convenient than integration of the radial distribution function over volume. Thus, the new approach might make these computations more accessible for practical applications. The insensitivity to system size is further encouraging in this regard. The fluctuation solution theory based on the KB integrals has already demonstrated its great potential, e.g., as winner of the third Industrial Fluid Properties Simulation Challenge in 2006.^{17,24}

4.2. Zeolite System. For the zeolite system, the embedded small system had sides dictated by the size of the crystallographic unit cell. The smallest system had sides $1/4L_{uc}$. The increments in small system size were 1/4 unit cell for each small system, and eight different small systems were used. Therefore, the largest small system embedded in the crystal is $2L_{uc}$, or 1/16th of the total simulation box.

In Figure 6, we plotted the inverse thermodynamic correction factor as a function of the loading. The solid line shows the values obtained from simulations in the grand-canonical ensemble with periodic boundary conditions, serving as a reference for the thermodynamic limit. The symbols are values obtained from embedding small systems in a canonical simulation, and the dashed lines are from embedding a small system of the same size in a grand-canonical simulation box. The overall correspondence is very reasonable. It is immediately clear that the shape of the

small system is very important for the result. All the small systems consisting of at least one unit cell in all directions correspond well with the result obtained from a system with periodic boundary conditions. For systems where this is not the case, the deviations are severe, and clearly deviate from the macroscopic result.

In Figure 7, we plotted the local density of one unit cell of silicalite-1, projected in the xy , xz , and yz -plane. Each point indicates the position of one single argon atom. The dashed lines indicate the 1/4 step in each direction. It is obvious that small changes in the shape of the small system have a large effect on the average number of particles inside the small system, and therefore, the fluctuations of energy and particles.

Figure 8 shows the isosteric heat of adsorption for argon in silicalite-1. Again, the reference values are plotted as a solid line, and the dashed lines are from embedding different small systems in the grand-canonical simulation. The symbols are from embedding the small system in a canonical ensemble. For lower loadings, all the small systems lead to good estimations of the molar isosteric heat of adsorption. The best approximation is found from the system with $L = 2L_{uc}$. The molar isosteric heat of adsorption does not seem to have the same strong dependence on the shape of the control volume, as the thermodynamic correction factor. However, it is significantly better to have a subvolume with sides being at least one single unit cell.

The zeolite system does not show a pronounced finite-size scaling of $1/L$ as was found for the homogeneous systems. We feel that this is most likely related to the zeolite structure. With that in mind, sampling in the canonical ensemble gives very good agreement, as long as the structure of the zeolite is taken into account.

5. CONCLUSION

In this work, we further verified the method of sampling small systems embedded in a large reservoir. We conclude that the proposed method leads to very good results and can be considered as a valuable tool in obtaining thermodynamic data for systems where it is difficult to perform simulations directly in the grand-canonical ensemble, e.g., at low temperature. Obtaining the Kirkwood–Buff integrals has been shown to be very efficient using this method, and one avoids the inherent problems associated with integrating the radial distribution function over volume. Moreover, the required system size is much smaller. This

is especially useful for studying dense systems, where simulations in the grand-canonical ensemble are too inefficient. The results for the zeolite system show that for heterogeneous systems the size of the control volume needs to be commensurate to the size of the unit cell of the zeolite. This is in agreement with the findings of Simon and Rubi²⁵ concerning local temperature fluctuations.

■ AUTHOR INFORMATION

Corresponding Author

*E-mail: signekj@nt.ntnu.no.

■ ACKNOWLEDGMENT

We acknowledge financial support from NWO-CW through an ECHO grant. Part of this work was performed as part of the Cluster of Excellence “Tailor-Made Fuels from Biomass”, which is funded by the Excellence Initiative by the German federal and state governments to promote science and research at German universities. This work was sponsored by the Stichting Nationale Computerfaciliteiten (National Computing Facilities Foundation, NCF) for the use of supercomputing facilities, with financial support from the Nederlandse Organisatie voor Wetenschappelijk onderzoek (Netherlands Organization for Scientific Research, NWO).

■ REFERENCES

- (1) Kjelstrup, S.; Bedeaux, D. *Non-equilibrium thermodynamics of heterogeneous systems*; World Scientific: Singapore, 2008.
- (2) Hill, T. L. *Thermodynamics of Small Systems, Part 1*; Benjamin: New York, 1963.
- (3) Schnell, S. K.; Vlugt, T. J. H.; Simon, J.-M.; Bedeaux, D.; Kjelstrup, S. *Chem. Phys. Lett.* **2011**, *504*, 199–201.
- (4) Binder, K. *Phys. Rev. Lett.* **1981**, *47*, 693–696.
- (5) Vlugt, T. J. H.; García Pérez, E.; Dubbeldam, D.; Ban, S.; Calero, S. *J. Chem. Theory Comput.* **2008**, *4*, 1107–1118.
- (6) Krishna, R.; Wesselingh, J. A. *Chem. Eng. Sci.* **1997**, *52*, 861–911.
- (7) Krishna, R. *J. Phys. Chem. C* **2009**, *113*, 19756–19781.
- (8) Floquet, N.; Simon, J. P.; Coulomb, J.-M.; Bellat, J. P.; Weber, G.; Andre, G. *Microporous Mesoporous Mater.* **2009**, *122*, 61–71.
- (9) Dubbeldam, D.; Calero, S.; Vlugt, T. J. H.; Krishna, R.; Maesen, T. L. M.; Smit, B. *J. Phys. Chem. B* **2004**, *108*, 12301–12313.
- (10) Kirkwood, J. G.; Buff, F. P. *J. Chem. Phys.* **1951**, *19*, 774–778.
- (11) Frenkel, D.; Smit, B. *Understanding Molecular Simulations*; Academic Press: New York, 2002.
- (12) Maginn, E. J. *J. Phys.: Condens. Matter* **2009**, *21*, 373101–373118.
- (13) Karavias, F.; Myers, A. L. *Langmuir* **1991**, *7*, 3118–3126.
- (14) Ruckenstein, E.; Shulgin, I. *Fluid Phase Equilib.* **2001**, *180*, 345–359.
- (15) Wedberg, R.; O’Connell, J. P.; Peters, G. H.; Adildskov, J. *Mol. Simul.* **2010**, *36*, 1243–1252.
- (16) Wedberg, R.; O’Connell, J. P.; Peters, G. H.; Adildskov, J. *Fluid Phase Equilib.* **2011**, *302*, 32–42.
- (17) Christensen, S.; Peters, G. H.; Hansen, F. Y.; O’Connell, J. P.; Abildskov, J. *Fluid Phase Equilib.* **2007**, *260*, 169–176.
- (18) Christensen, S.; Peters, G. H.; Hanse, F. Y.; O’Connell, J. P.; Abildskov, J. *Mol. Simul.* **2007**, *33*, 449–457.
- (19) Nichols, J. W.; Moore, S. G.; Wheeler, D. R. *Phys. Rev. E* **2009**, *80*, 051203.
- (20) Weeks, J. D.; Chandler, D.; Andersen, H. C. *J. Chem. Phys.* **1971**, *54*, 5237–5247.
- (21) Allen, M. P.; Tildesley, D. J. *Computer Simulation of Liquids*; Clarendon Press: Oxford, U.K., 1987.
- (22) García-Pérez, E.; Parra, J. B.; Ania, C. O.; Dubbeldam, D.; Vlugt, T. J. H.; Castillo, J. M.; Merkling, P. J.; Calero, S. *J. Phys. Chem. C* **2008**, *112*, 9976–9979.
- (23) Baerlocher, C.; McCusker, L. B.; Olson, D. H. *Atlas of Zeolite Framework Types*, 6th ed.; Elsevier: Amsterdam, 2007.
- (24) <http://fluidproperties.org/challenge/3rd/results>.
- (25) Simon, J. M.; Rubi, J. M. *J. Phys. Chem. B* **2011**, *115*, 1422–1428.